Noise Model of InP–InGaAs SHBTs for RF Circuit Design

A. Huber, *Member, IEEE*, D. Huber, *Student Member, IEEE*, C. Bergamaschi, *Member, IEEE*, T. Morf, *Member, IEEE*, and H. Jäckel, *Member, IEEE*

***Abstract*—A scalable small-signal and noise model of InP–InGaAs single heterojunction bipolar transistors was developed. Effects which become important at higher frequencies such as the correlation between base and collector current noise and frequency-dependent base current noise are taken into account. We will show that these effects are significant at frequencies higher than 40 GHz and can no longer be neglected. Our model also includes the effects of the different emission coefficients of the base and collector currents. Using this improved model, a direct-coupled, lumped broad-band amplifier was designed. We completely characterized the fabricated circuit with respect to small-signal, noise, and linearity behavior. A −3-dB bandwidth of 50 GHz with a dc gain of 9.8 dB and a gain-peaking of only 1.2 dB were achieved. All these values agree very well with the simulation results. The noise figure is 7.5 dB over a large frequency range. In the frequency range from 2 to 50 GHz, the third-order intercept point IP_3 and 1-dB compression point at the output have values from 17 to 10 dBm and 3 to 0 dBm, respectively.**

***Index Terms*—Broad-band amplifiers, feedback amplifiers, heterojunction bipolar transistor, high-frequency noise, InP, low-frequency noise, noise model.**

I. Introduction

THE transmission capacity of fiber-optical communications systems and the number of wireless applications in the millimeter-wave range have increased rapidly. High-speed electronic circuits are required for the transmission and processing of data with rates in the multigigabit per second range. In a transmission system, not only high data rates, but also the sensitivity especially of the receiver front-ends are of interest because it limits the maximal distance between two regeneration circuits, affecting directly the cost of the system. The sensitivity is related to the noise behavior of the receiver circuit which is determined by the noise performance of the transistors and resistive elements. For the design of the electronic circuits in the transmission systems, we need a transistor technology that can handle the high data rates of 40 Gb/s and more. Additionally, accurate models of these transistors have to be developed, which also include the noise sources.

Transistor technologies using III–V semiconductor are the most promising candidates to meet the speed requirements because of the excellent transport properties of the materials employed. Heterojunction bipolar transistors (HBTs) [1]–[5] and high electron mobility transistors (HEMTs) [6] realized in different material systems have been developed. The high-speed capability was demonstrated for all these technologies. Considering the noise behavior, HEMTs are generally superior to HBTs in noise matched situations. However, the best values of reported sensitivities of photoreceivers are comparable.

Classical models of HBTs have serious deficiencies when applied to the microwave regime, especially if the noise properties of the devices are not modeled exactly. For example, often the collector delay and the correlation between the base and collector noise currents are not included in the models. However, models exist that take this correlation into account [7], [8] and even consider the bias and temperature dependence of the model elements [9]–[11]. All these models operate with frequency-independent noise sources although they were either developed for the investigation of the noise properties of the HBT or for the design of low-noise circuits in the microwave range. In this paper, we will demonstrate that the variation of the power spectral densities of the noise sources with frequency may become important when the operating frequencies are extended to 40 GHz and higher. Present noise models which include frequency-dependent noise sources [12] nevertheless neglect the correlation between the base and collector noise current.

For the design of noise-optimized oscillators, it is important that the low- and high-frequency noise sources are included in the same model. However, the low-frequency noise sources are often missing in models of HBTs developed for the microwave range [13]. On the other hand, noise models which are used to investigate the noise behavior in the low-frequency range [14]–[16] do not take the microwave noise into account.

In this paper, we report on a scalable small-signal and noise model of our InP–InGaAs SHBTs which takes the significant effects of the correlation between the base and collector current noise and the frequency dependence of the base noise source into consideration. This frequency dependence is relevant at frequencies below the $1/f$ corner frequency ($<$10 MHz) and in the very high-frequency range ($>$40 GHz). Using this model, we designed a broad-band amplifier which was fabricated and completely characterized showing good agreement in all parameters with the simulations.

II. Technology

The InP–InGaAs SHBTs used for modeling and subsequently for the amplifier design have a MOVPE-grown layer structure and a self-aligned emitter as described comprehensively in [17]. The thicknesses of the base and collector range from 50 to 80 nm

Manuscript received November 10, 2000; revised September 16, 2001.

A. Huber was with the Electronics Laboratory, Swiss Federal Institute of Technology Zürich (ETHZ), CH-8092 Zürich, Switzerland. He is now with Zentrum für Mikroelektronik, FH Aargau, CH-5210 Windisch, Switzerland.

D. Huber and H. Jäckel are with the Electronics Laboratory, Swiss Federal Institute of Technology Zürich (ETHZ), CH-8092 Zürich, Switzerland.

C. Bergamaschi is with Zentrum für Mikroelektronik, FH Aargau, CH-5210 Windisch, Switzerland.

T. Morf is with IBM Rüschlikon, CH-8803 Rüschlikon, Switzerland.

Publisher Item Identifier 10.1109/TMTT.2002.800384.

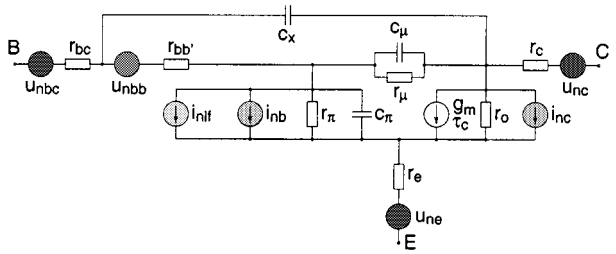

Fig. 1. Equivalent small-signal model with the current noise sources i_{nx} and the thermal noise sources u_{nx}.

and from 400 to 800 nm, respectively. These devices achieve a dc current gain β between 20 and 50. The values of f_T and $f_{\max}$ were extrapolated from on-wafer S-parameter measurements up to 110 GHz. At a collector current density of 130 kA/cm^2 and a collector–emitter voltage of 2 V, maximum f_T and $f_{\max}$ reach 130 and 220 GHz, respectively. Resistors are made of evaporated Cr-films having a sheet resistance of 50 $\Omega/\square$. The capacitors are formed by the base–collector depletion capacitance. A passivation layer of polyimide additionally serves for planarization.

III. Noise Model

For circuit design and even more for the optimization of the circuits with respect to noise, noise models of the devices are needed. Measurement data and equations from the device physics serve to develop these models. Since we do not aim at a completely physical model which is often too complex for circuit design, we base our transistor model, shown in Fig. 1, on the commonly used small-signal π-model combined with the necessary noise sources.

The forward-biased base–emitter diode is modeled by the small-signal resistance r_π and capacitance c_π. r_π is given by $n_B V_T/I_B$, where I_B is the dc base current, n_B its ideality factor, and V_T, the thermal voltage. c_π is the sum of the diffusion capacitance c_D and the capacitance c_{je} of the forward-biased junction. The base–emitter voltage controls the collector current via the intrinsic transconductance $g_m = g_{m0} \cdot \exp(j\omega\tau_C)$, where $g_{m0} = I_C/(n_F V_T)$. I_C and n_F denote the dc collector current and its ideality factor, respectively. τ_C is the collector delay which is obtained from the expression $\tau_C = X_C/(2v_{\text{sat}})$, where X_C is the collector thickness and v_{sat} denotes the electron saturation velocity. c_μ and c_x are the intrinsic and extrinsic base collector capacitances, respectively. r_μ models the leakage currents of the base collector junction. The current noise sources of the base (i_{nb}) and collector (i_{nc}) as well as the low-frequency noise sources i_{nlf} are also included. Section III-A describes these noise sources in detail. The ohmic series resistances between the device terminals and the active device are modeled by the base ($r_{bb'}$), (r_{bc} for the contact), the collector (r_c), and the emitter (r_e) resistors. The two parameters r_e and r_c are the bulk resistances of the emitter and subcollector, respectively. For the calculation of the internal base resistance, we take the effects of the inhomogeneous lateral current flow within the base into account [18], which results from the voltage drop in the base along the base–emitter junction. The external base resistance, including the contact resistance, is determined using the analogy to the transmission-line model [19]. Associated with the series resistances are the thermal noise sources u_{nbb}, u_{nbc}, u_{nc}, and u_{ne}. The power spectral densities of the thermal noise sources are directly related with the resistances via the well-established relation $\overline{u_n^2} = 4kTR$.

The small-signal parameters are determined by fitting the model parameters to the measured S-parameters and noise parameters. During the fitting procedure, the parameters r_π, c_D, and g_m were fixed at their calculated values. The remaining parameters were variable since they are modified by inhomogeneous field distributions, which are difficult to predict, or by uncertainties in the exact geometric shapes, for example, due to under-etching of the base contact.

A. Current Noise Sources

Our noise model consists of the three current noise sources i_{nb}, i_{nc}, and i_{nlf}. First, the power spectral densities of i_{nb} and i_{nc} are calculated. To do this, we assume that the electron transport through the base is limited by the diffusion processes in the base itself and not by the carrier injection from the heterojunction. This assumption is valid since the ballistic transport mechanisms should not dominate for the base thicknesses of our devices which are larger than 50 nm [20], [21]. The processes in the base which have to be considered are therefore diffusion and bulk recombination. The resulting continuity equations consist of the lifetime of the minority carriers and of their diffusion constant in the base. The values of these physical properties of our HBTs were determined in a previous work [5]. Using the analogy between these continuity equations and the equations of the signal propagation on a lossy transmission line, the power spectral densities of the equivalent noise sources were calculated [22]. We therefore have to transform all the microscopic noise sources of the diffusion and recombination processes within the base to the edges of the base region. This transformation leads to a distributed problem for the calculation of the power spectral densities of the base and collector current noise sources. To solve this problem, we implemented the transmission line with the line segments comprising the microscopic noise sources into a circuit simulator. As a result of our simulation, we obtained the power spectral densities of the base and collector current noise sources which we normalized to the conventional shot noise formula: $C_{bb} = \overline{i_{nb}^2}/(2qI_B)$ and $C_{cc} = \overline{i_{nc}^2}/(2qI_C)$. These normalized quantities are shown in Fig. 2 for base thicknesses from 50 to 100 nm.

Full shot noise, i.e., both C_{bb} and C_{cc} equal unity, can be observed at relatively low frequencies. At higher frequencies, the collector current noise still shows shot noise whereas the base noise significantly increases by about 50% at 40 GHz. This behavior can be explained as follows. At lower frequencies, the electrons are injected from the emitter into the base where they are collected by the collector or where they recombine. At higher frequencies, some fluctuating electrons return to the emitter before they recombine or before they enter the collector. These returning electrons lead to the increased base current noise but do not modify the collector current noise [23].

In addition to the frequency dependence of the base noise source, the model also includes the correlation between the base and collector noise currents. This correlation was also

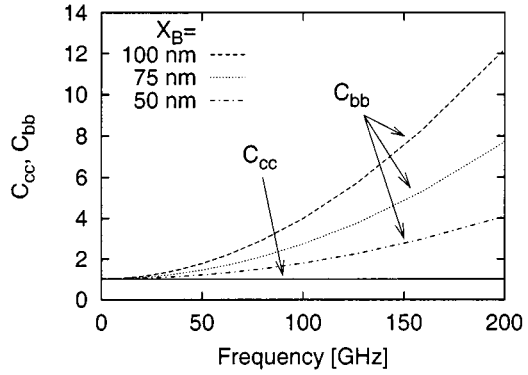

Fig. 2. Normalized power spectral noise densities $C_{bb} = \overline{i_{nb}^2}/(2qI_B)$ and $C_{cc} = \overline{i_{nc}^2}/(2qI_C)$ of the base and collector, respectively, for base thicknesses X_B from 50 to 100 nm, $\tau_n = 20$ ps, and $D_n = 44$ cm^2/s.

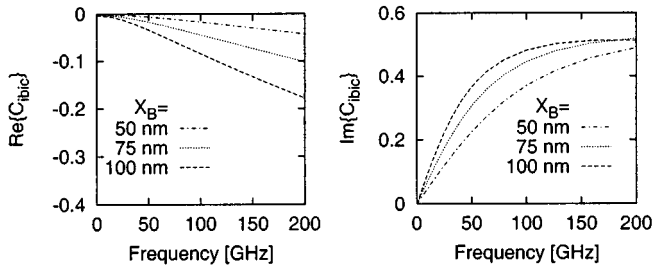

Fig. 3. Real and imaginary parts of the correlation coefficient C_{ibic} of the base and collector noise current for base thicknesses X_B from 50 to 100 nm, $\tau_n = 20$ ps, and $D_n = 44$ cm^2/s.

analyzed using the transmission-line model. The resulting frequency dependence is depicted in Fig. 3 for base thicknesses ranging from 50 to 100 nm. The real and imaginary parts of the correlation factor C_{ibic} deviate from zero at higher frequencies. As we could already observe for the base current noise, the frequency dependence is stronger for thicker bases. We will see in Section IV-A that C_{ibic} is not negligible in high-frequency circuits.

The collector delay τ_C, which was not taken into account in the above calculations, results in an additional delay modifying the base noise source and the correlation. Furthermore, the different emission coefficient of the base and collector currents observed in HBTs, which are often neglected in noise models [24], [13], affect the noise behavior of the transistor [25]. Combining these effects with the analytical expressions which fit the simulation results well for the equivalent noise sources originating from the noise in the base (Figs. 2 and 3), we obtain

$$\overline{i_{nb}^2} = 2qI_E \left|\frac{c_e}{c_{e0}}\right|^2 - 2qI_C \left|\frac{c_c n_e}{c_{c0} n_F}\right|^2 - 2qI_E \left|\frac{c_e}{c_{c0}} - 1\right|^2 + 2qI_C \left|\frac{c_c n_e}{c_{c0} n_F}\, e^{-j\omega\tau_C} - 1\right|^2 \quad (1)$$

$$\overline{i_{nc}^2} = 2qI_C \quad (2)$$

$$\overline{i_{nb}^* i_{nc}} = 2qI_C \left(\frac{c_c n_e}{c_{c0} n_F}\, e^{-j\omega\tau_C} - 1\right) \quad (3)$$

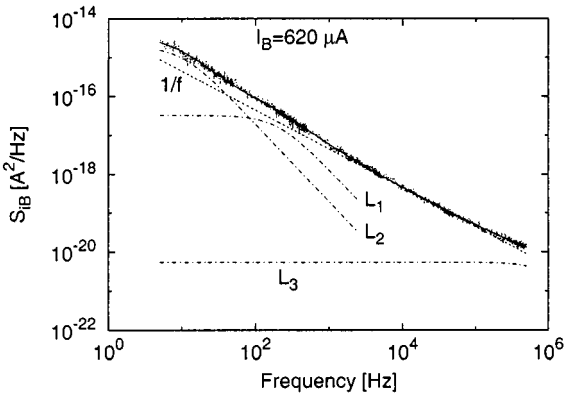

Fig. 4. Power spectral density of the low-frequency noise for an HBT with 2.5 $\times$ 8 μm^2 at a base current of 620 μA in the frequency range from 5 Hz to 500 kHz. The spectrum is decomposed into a $1/f$ and three different Lorentzian components ($L_1 \cdots L_3$).

where

$$n_e = \frac{\beta n_F + n_B}{1+\beta}$$

and n_F and n_B are the emission coefficients of the collector and base currents, respectively. The formulas for c_e, c_{e0}, c_c, and c_{c0} are found in the Appendix. Equations (1)–(3) correspond to van der Ziel's theory [22], whereas the effects of the collector delay and the different emission coefficient of the base and collector currents are included additionally. These equations are implemented into the hybrid π-model (Fig. 1) for circuit simulation.

The model of the low-frequency noise source (i_{nlf}) was determined from measurements. We measured the power spectral voltage density at the collector using a low-noise amplifier (SR 560) and a vector signal analyzer (HP 89 441A). This voltage was transformed into an equivalent noise current at the base. Fig. 4 represents the power spectral density of the base noise current in the frequency range from 5 Hz to 500 kHz for an HBT with an emitter area of 2.5 $\times$ 8 μm^2 at a base current of 620 μA. The low-frequency power spectral noise current density of the base current was fitted to an expression consisting of a $1/f$-part ($S_{1/f}$), a sum of Lorentzian type spectra (L_i), and a component showing white noise

$$\overline{i_{nlf}^2} = \frac{B_0}{f} + \sum_{i=1}^{3} \frac{B_i}{f_{0,i}} \frac{1}{1+\left(\frac{f}{f_{0,i}}\right)^2}. \quad (4)$$

Equation (4) is often used for the characterization of low-frequency noise [26] and has already been found to be well suited for InP–InGaAs HBTs [27].

For circuit design as well as to localize and identify the noise sources in the HBT, the dependences of the power spectral density of the base noise current upon the base current I_B and the ratio of the emitter perimeter to emitter area P_E/A_E are useful to know. The analysis of these dependences showed a $1/f$ component (B_0) which linearly depends on I_B and which is independent of P_E/A_E. This behavior is typical for noise originating from bulk effects, e.g., fluctuation in the diffusion

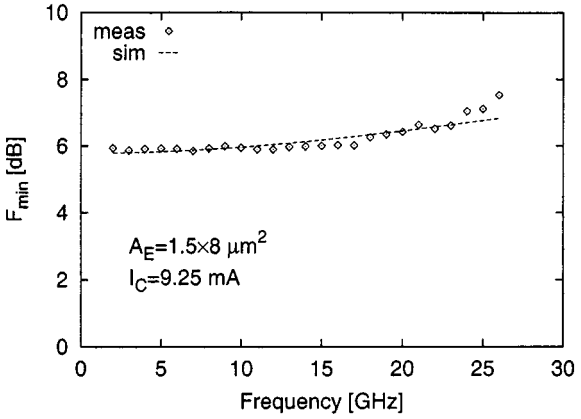

Fig. 5. Measured (◇) and simulated (—) minimum noise figures $F_{\min}$ of an HBT with $A_E = 1.5 \times 8\ \mu\text{m}^2$, $I_C = 9.25$ mA from 2 to 26 GHz.

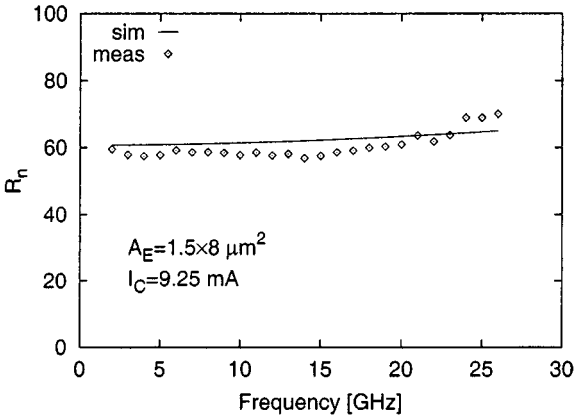

Fig. 6. Measured (◇) versus simulated (—) noise resistance R_n of an HBT with $A_E = 1.5 \times 8\ \mu\text{m}^2$ and $I_C = 9.25$ mA.

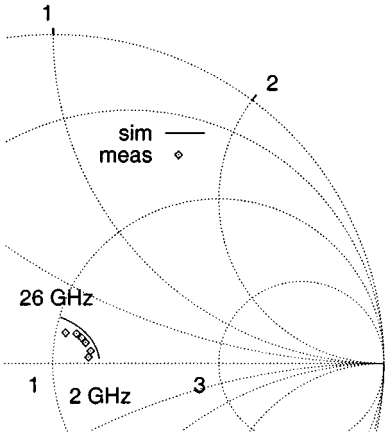

Fig. 7. Measured and simulated optimum source reflection factor Γ_{opt} at $I_C = 9.25$ mA and $A_E = 1.5 \times 8\ \mu\text{m}^2$.

TABLE I
EQUIVALENT CIRCUIT PARAMETERS OF THE MODEL FOR AN HBT WITH $A_E = 1.5 \times 8\ \mu\text{m}^2$, AT $I_C = 9.25$ mA AND $V_C = 1.5$ V

parameter	fit	calculated	unit
$r_{bb'}$	28.8	$R_B = 30.1$	[Ω]
r_{bc}	0	$= r_{bb'} + r_{bc}$	
r_E	3.8	2.7	[Ω]
r_C	4.1	5.5	[Ω]
r_π	74.9	74.9	[Ω]
$c_\pi\ (= c_D + c_{je})$	407	$c_D = 347$	[fF]
c_{je}	60		[fF]
g_m	255	255	[mS]
c_μ	5.5	$C_{BC} = 12.4$	[fF]
c_{bcx}	8.4	$= c_\mu + c_{bcx}$	
r_μ	40		[kΩ]
r_0	10		[kΩ]

constant [28], rather than from surface recombination. Surface recombination would lead to a quadratic dependence upon the base current and the P_E/A_E which was actually observed for the parameters B_i, the generation-recombination components.

B. Comparison of the Measurement Versus Model

In order to test the quality of our model, we compared the measurement data of the noise parameters with the simulations using our model [29], [30] but with the addition of the frequency dependence and correlation coefficient of the noise sources calculated in Section III-A. The results for an HBT having an emitter area of $1.5 \times 8\ \mu$m are given in Figs. 5–7 for the minimum noise figure $F_{\min}$, R_n, and Γ_{opt}, respectively. We can observe a very good agreement for all three noise parameters in the frequency range from 2 to 26 GHz (limits of the noise parameter measurement system). Since some of the model parameters are fitted, we have to verify if these parameters are reasonable. The values of the parameters after fitting are therefore compared in Table I with calculated values. The fitted values correspond well with the calculated values obtained from the theoretical analysis in Section III. This demonstrates that our model is useful and consistent for InP-HBTs in the microwave range.

For the circuit design and optimization, some model parameters ($r_\pi, g_m, c_D, i_{nb}, i_{nc}$) are bias-dependent. In order to control the accuracy of the bias dependence, the model elements were fitted only in one bias point ($I_C = 2$ mA and $V_C = 1.5$ V). Then, the bias conditions were varied without further fitting steps. The solid curve in Fig. 8 shows the simulated minimum noise figure at 10 GHz for a device having an emitter area of $1.5 \times 8\ \mu\text{m}^2$ operated in the collector current range from 0.3 to 9.5 mA. The good agreement between measurement and simulation proves the quality of our model in a large range of the collector current.

A more difficult task than modeling the bias dependence is to develop a model which is scalable with geometry because parasitic capacitances or inhomogeneous field distributions do not scale via a simple relation with the emitter area. In Fig. 9, the simulated and measured minimum noise figure for different emitter width W_E and emitter length L_E are shown for constant collector current density J_C.

The minimum noise figure increases with a larger emitter width mainly due to the enlargement of the internal base resistance. However, for emitter widths smaller than 1.5 μm, the reduction of $F_{\min}$ is less pronounced because the deterioration of the current gain almost compensates for the influence of the reduced base resistance.

At a constant collector current density, $F_{\min}$ remains almost constant in the range of the investigated emitter length. The de-

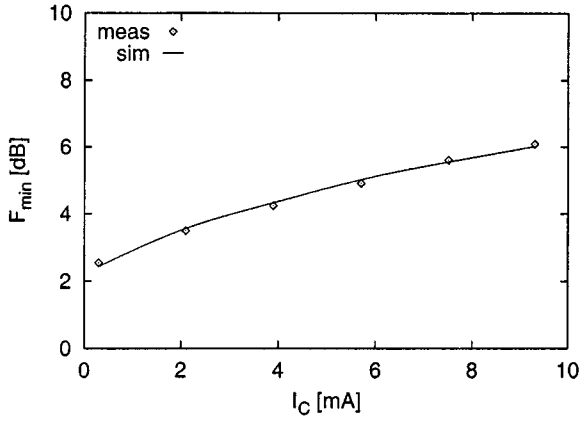

Fig. 8. Comparison between the simulated and measured minimum noise figure $F_{\min}$ of a device with $A_E = 1.5 \times 8\ \mu\text{m}^2$ at 10 GHz.

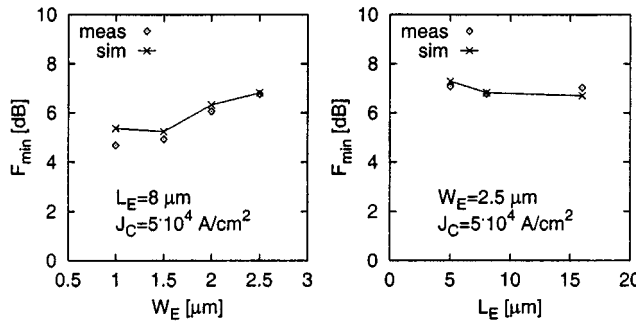

Fig. 9. Simulated and measured $F_{\min}$ versus emitter width W_E and emitter length L_E at $J_C = 5 \cdot 10^4$ A/cm^2 and $f = 10$ GHz.

crease of the minimum noise figure caused by the reduced base resistance of long emitter devices is canceled by the higher current noise.

We observe good agreement especially for large devices. However, for smaller device structures, the difference between measurement and simulation becomes more pronounced. For example, for a $1.0 \times 8\ \mu\text{m}^2$ HBT, the simulated minimum noise figure is 20% higher than the measured one. The larger disagreement for smaller devices can be explained by the fact that influences of parasitics as well as fabrication tolerances are more pronounced and difficult to model exactly.

For the selection of the device size and bias point, an investigation of the relative contribution of each noise source to the overall noise power is helpful. The results for different device sizes operated at two different collector current densities are presented in Table II. At small currents ($J_C = 1.75 \cdot 10^4$ A/cm^2), the thermal noise sources of the series resistances constitutes 40% and the current noise sources 60% of the total noise power. At higher currents ($J_C = 7.75 \cdot 10^4$ A/cm^2), the current noise dominates even more (80%). Since the base current is the most dominant noise source (60%), transistors with high current gains are required for low-noise designs. This can, for example, be reached by a variation of the emitter orientation with respect to the InP crystal. Because of the fact that the etching behavior depends on the crystal orientation, the emitter undercut can be increased, leading to a substantially higher current gain [31].

TABLE II
RELATIVE NOISE CONTRIBUTION OF THE NOISE SOURCES TO THE OUTPUT NOISE POWER AT 10 GHz IN A 50-Ω ENVIRONMENT

A_E [μm^2]	J_C [A/cm^2]	u_{nb}	u_{ne}	u_{nc}	i_{nb}	i_{nc}
1.0 × 8	1.75·10^4	28 %	15 %	0 %	30 %	27 %
	7.75·10^4	16 %	5 %	0 %	63 %	16 %
1.5 × 8	1.75·10^4	32 %	10 %	0 %	31 %	27 %
	7.75·10^4	21 %	5 %	0 %	57 %	17 %
2.5 × 8	1.75·10^4	37 %	4 %	0 %	40 %	19 %
	7.75·10^4	17 %	1 %	0 %	61 %	21 %

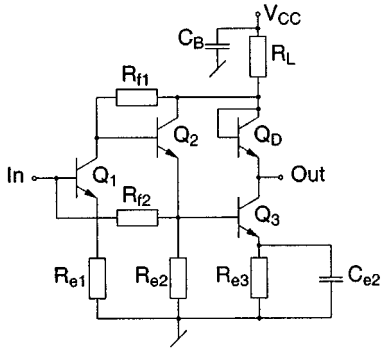

Fig. 10. Schematic of the direct-coupled dual-feedback amplifier.

IV. AMPLIFIER DESIGN

In this section, the design of a dual-feedback ultrabroad-band Darlington amplifier is described [32], [33]. This design serves to verify that our model is indeed useful for the design of RF circuits. Furthermore, it demonstrates the potential of the InP-HBT technology for the highest frequency applications.

The amplifier topology shown in Fig. 10 has originally been demonstrated in [34] for Si-BJT low-noise amplifiers. The circuit consists of two gain stages where the first stage is a common emitter stage, Q_1, and the second stage a Darlington amplifier, Q_2 and Q_3, with a series feedback resistor R_{e2} and shunt feedback resistor R_{f1}. The resistor R_{e1} serves for biasing the transistor Q_2. By adjusting the resistor R_L, optimal output power match to 50 Ω and maximal power gain was obtained. The gain-bandwidth characteristic of the Darlington stage has been optimized by changing the series and parallel feedback resistors R_{e2} and R_{f1}, respectively. The multiple feedback topology makes it possible to simultaneously optimize also the input return loss by varying the shunt feedback resistor R_{f2} without degrading the gain bandwidth performance severely.

Fig. 11 shows the chip photograph of the amplifier. The total chip size is $550 \times 640\ \mu\text{m}^2$ which is mainly determined by the available pad frame. The three contact pads at the left, the right and at the top of the chip are the input, output and supply voltage pads, respectively. A 12 pF blocking capacitor is introduced for stabilizing the supply voltage. All transistors of the circuit have the same emitter size of $1.0 \times 8\ \mu\text{m}^2$. They are not individually optimized.

A. Measured Results

The RF S-parameters were measured on-wafer from 0.045 to 75 GHz. The amplitude and phase of S_{21} and the group delay

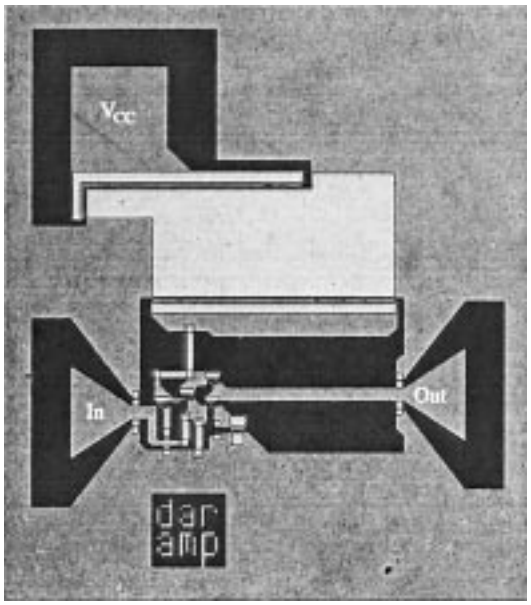

Fig. 11. Chip photograph of the amplifier using a chip area of $550 \times 640\ \mu\text{m}^2$.

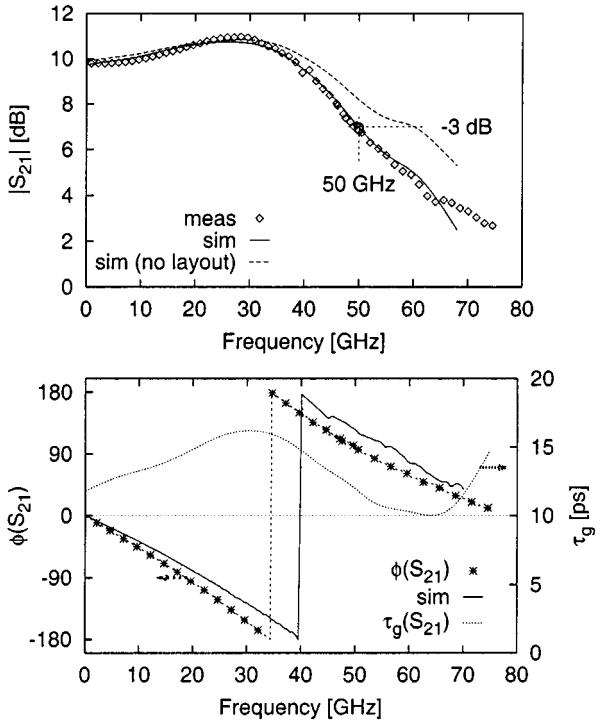

Fig. 12. Measured and simulated amplitude, phase ϕ (—), and group delay τ_g (- -) of S_{21} in the frequency range from 0.045 to 75 GHz.

are depicted in Fig. 12. At a supply voltage of 10 V, the amplifier reaches a gain of 9.8 dB and a -3 dB-bandwidth of 50 GHz. These results are comparable with other HBT amplifier circuits [35], [36]. A problem which often occurs using feedback amplifiers is a gain peak in the frequency response. In our design, this peak could almost be suppressed completely. The gain-peaking remains below 1.2 dB which is considerably lower than in other published investigations with similar gain-bandwidth performances.

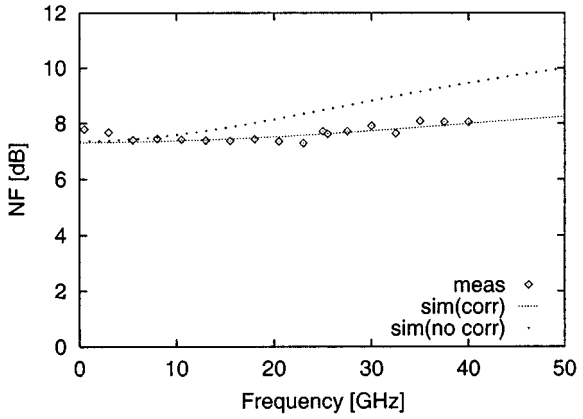

Fig. 13. Measured and simulated noise figure, with and without taking the correlation into account.

For the transmission of digital or pulse signals, a linear phase characteristic, corresponding to a constant group delay, is required. The group delay which is defined as

$$\tau_g = \frac{d\phi}{d\omega} \tag{5}$$

is a measure for the signal dispersion. The value of τ_g equals 12.5 ps and is almost constant with a variation of only ± 2.5 ps. Using the measured S-parameter data of the amplifier, time-domain simulations lead to an overshoot in the step response of about 7% only.

Very good agreement between simulation and measurement is only achieved if all the influences of the layout are taken into account. Without considering the layout parasitics, an overestimation of the bandwidth of more than 10 GHz is observed. Input and output return losses better than -12 dB for S_{11} and -13 dB for S_{22} are measured up to 50 GHz. Below 25 GHz, the values are even better than -20 dB. Thus, the amplifier provides very good power matching properties.

In Fig. 13, the measured and simulated noise figure is depicted in the frequency range from 2 to 41 GHz which is the frequency range where the noise figure measurement is within a tolerance of 0.5 dB. In this range, the noise figure remains between 7.5 and 8 dB. In order to investigate the influence of the correlation between the base and collector noise current, we carried out two types of simulations. One simulation takes the correlation into account and the other neglects it. At 40 GHz, the simulation disregarding the correlation predicts a noise figure which is 1.5 dB above the measured value, whereas the simulation with the correlation agrees excellently with the measurement. This demonstrates the importance of taking the correlation between the base and collector noise current into account. The frequency dependence of the power spectral density of the base noise current is not significant but is necessary for the calculation of the correlation.

We also analyzed the relative contributions of the different noise sources in the Darlington amplifier to the overall noise figure F. From the simulations, the results listed Table III were obtained, where r_b and r_e are the total base resistance and the emitter series resistance, respectively. I_B and I_C denote the base and collector currents of the input transistor, and R_{f1} and R_{f2} are the two feedback resistors of the amplifier. We can see that

TABLE III
RELATIVE NOISE CONTRIBUTION OF THE DIFFERENT NOISE SOURCES IN THE DARLINGTON AMPLIFIER

HBTs	Q_1	r_b	16 %	54 %	69 %
		r_e	4 %		
		$2qI_B$	29 %		
		$2qI_C$	5 %		
	Q_2			10 %	
	remaining transistors			5 %	
passive network	R_{e1}			13 %	31 %
	R_{f1}			6 %	
	R_{f2}			4 %	
	other passive elements			8 %	

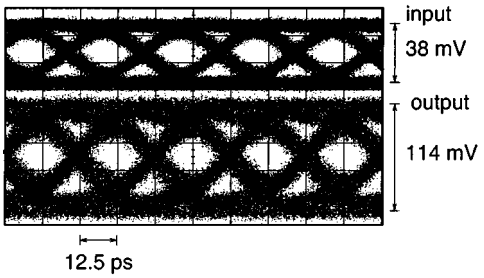

Fig. 14. Eye diagrams at the input and output of the amplifier for a 40-Gb/s PRBS of the length $2^{31}-1$.

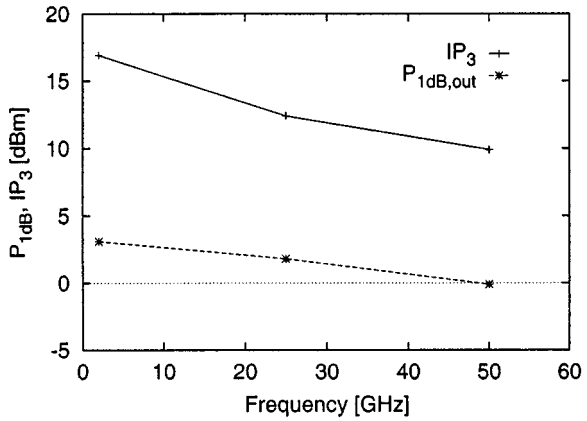

Fig. 15. Measured output powers of the third-order intercept point and 1-dB compression point at 2, 25, and 50 GHz.

more than two thirds (69%) of the noise originates from the active elements in the circuit and the rest (31%) from the passive network. We further observe that the most dominant noise contributions (54%) are caused by the noise sources of the first HBT Q_1. These results correspond well with Friss' formula [37] which states that the first amplifying stage contributes dominantly to the overall noise. The main noise source is the base current noise sources, which makes up 29% of the overall noise. Hence, transistors with high current gains, which reduce the base currents, are a requisite for low-noise amplifiers.

Fig. 14 shows a 40-Gb/s eye diagram of the amplifier. The setup for the eye diagram measurement is similar to the one described in [38] where the electrical 40-Gb/s NRZ signal was generated by electrically multiplexed 10-Gb/s signals. The opened eye diagram for a PRBS of the length $2^{31}-1$ at a data rate of 40 Gb/s demonstrates the operation of the amplifier without any ringing, overshoot, or signal jitter. However, the noise contribution of the amplifier decreases the open eye area.

Depending on the application, the linearity of the amplifier is of great importance as well. Therefore, we measured the third-order intercept point IP_3 and the output power at the 1-dB gain compression point as a function of the frequency. As shown in Fig. 15, IP_3 varies from 17 dBm at 2 GHz to 10 dBm at 50 GHz. In the same frequency range, the 1-dB compression at the output changes from 3 dBm to 0 dBm corresponding to an output voltage swing of 890 mV_{p-p} and 630 mV_{p-p}, respectively.

V. CONCLUSION

A scalable small-signal and noise model of InP–InGaAs single heterojunction bipolar transistors (SHBT) based on the hybrid π-model was presented. We analyzed the noise behavior using the analogy between a lossy transmission line and the transport processes in the base. As a result, we obtain a frequency-dependent base current noise and a correlation between the base and the collector current noise sources. This correlation effect becomes important at frequencies above $\simeq$40 GHz. We demonstrate good agreement between the measured and simulated noise parameters.

Our noise model enabled us to design a monolithic, direct-coupled feedback amplifier. The fabricated circuit exhibit a very flat gain of 9.8 dB and a bandwidth of 50 GHz. With input and output return losses better than -12 and -13 dB, respectively, the amplifier has excellent power matching properties. We demonstrated the operation of the amplifier at 40 Gb/s whereas the bandwidth, in combination with the linear phase, should be sufficient for $>$60-Gb/s data transmission. In addition, the data from the measurements correspond very well with the simulations which proves the quality and validity of our model for RF circuit design.

APPENDIX

Formulas for c_e, c_{e0}, c_c, and c_{c0} used to describe the equations of the power spectral densities of the noise sources [see (1)–(3)] in Section III-A

$$c_e = \frac{\gamma X_B}{\tanh \gamma X_B} \quad c_{e0} = c_e(\omega = 0)$$

$$c_c = \frac{\gamma X_B}{\sinh \gamma X_B} \quad c_{c0} = c_c(\omega = 0).$$

γ is the propagation constant in the base and is given by

$$\gamma = \frac{1}{\sqrt{D_n \tau_n}} \sqrt{1 + j\omega\tau_n}$$

where D_n is the diffusion constant, τ_n is the electron lifetime in the base, and X_B is the base thickness.

ACKNOWLEDGMENT

The authors would like to thank the staff of the Microelectronics and Optoelectronics Laboratory of the ETHZ for the opportunity to use their clean room facilities and especially R. Bauknecht for material growth. They further acknowledge the Fraunhofer Institute of Applied Solid State Physics, Freiburg, Germany, where they had the possibility to measure

the 40-Gb/s eye diagrams. Thanks also go to H. R. Benedickter, Laboratory for Electromagnetic Fields and Microwave Electronics of the ETHZ, for his continuous support during RF measurements.

REFERENCES

[1] K. Rungei, P. J. Zampardi, R. L. Pierson, P. B. Thomas, S. M. Beccue, R. Yu, and K. C. Wang, "High speed AlGaAs/GaAs HBT circuits for up to 40 Gb/s optical communication," in *IEEE GaAs IC Symp.*, 1997, pp. 211–214.

[2] M. Rodwell, J. F. Jensen, W. E. Stanchina, R. A. Metzger, D. B. Rensch, M. W. Pierce, T. V. Kargodorian, and Y. K. Allen, "33-GHz monolithic cascode AlInAs/GaInAs heterojunction bipolar transistor feedback amplifier," in *IEEE Bipolar Circuits and Technology Meet.*, Sept. 1990, pp. 252–255.

[3] J. Müllrich, T. F. Meister, M. Rest, W. Bogner, A. Schöpflin, and H.-M. Rein, "40 Gbit/s transimpedance amplifier in SiGe bipolar technology for the receiver in optical-fiber TDM links," *Electron. Lett.*, vol. 34, pp. 452–453, Mar. 1998.

[4] Q. Lee, S. C. Martin, D. Mensa, R. P. Smith, J. Guthrie, and M. J. W. Rodwell, "Submicron transferred-substrate heterojunction bipolar transistor," *IEEE Electron Device Lett.*, vol. 20, pp. 396–398, Aug. 1999.

[5] R. Bauknecht, "InP double heterojunction bipolar transistors for driver circuits in fiber optical communication systems," Ph.D. dissertation, ETH Zürich, Zürich, Switzerland, 1998.

[6] P. M. Smith, "Status of InP HEMT technology for microwave receiver applications," in *IEEE Microwave and Millimeter-Wave Monolithic Circuits Symp.*, 1996, pp. 129–132.

[7] L. Escotte, J. P. Roux, R. Plana, J. Graffeuil, and A. Gruhl, "Noise modeling of microwave heterojunction bipolar transistor," *IEEE Trans. Electron Devices*, vol. 42, pp. 883–889, May 1995.

[8] J.-P. Roux, L. Escotte, R. Plana, J. Graffeuil, S. L. Delage, and H. Blanck, "Small-signal and noise model extraction technique for heterojunction bipolar transistor at microwave frequencies," *IEEE Trans. Microwave Theory Tech.*, vol. 43, pp. 293–297, Feb. 1995.

[9] R. A. Pucel, T. Daniel, A. Kain, and R. Tayrani, "A bias and temperature dependent noise model of heterojunction bipolar transistors," in *IEEE MTT-S Int. Microwave Symp. Dig.*, 1998, pp. 141–144.

[10] H. Dodo, Y. Amamiya, T. Niwa, M. Mamada, S. Tanaka, and H. Shimawaki, "Microwave low-noise GaAs HBTs," in *IEEE MTT-S Int. Microwave Symp.*, 1998, pp. 1–4.

[11] T. Daniel, "Bias and temperature dependent noise modeling of HBTs," in *IEEE MTT-S Int. Microwave Symp. Dig.*, 1997, pp. 1469–1472.

[12] J. J. Liou, T. J. Jenkins, L. L. Liou, R. Neidhard, D. W. Barlage, R. Fitch, J. P. Barrette, M. Mack, C. A. Bozada, R. H. Y. Lee, R.-W. Dettmer, and J. S. Sewell, "Bias, frequency, and area dependencies of high frequency noise in AlGaAs/GaAs HBTs," *IEEE Trans. Electron Devices*, vol. 43, pp. 116–122, Jan. 1996.

[13] M. Rudolph, R. Doerner, L. Klapproth, and P. Heymann, "An HBT noise model valid up to transit frequency," *IEEE Electron Device Lett.*, vol. 20, pp. 24–26, 1999.

[14] Y. Takanashi and H. Fukano, "Low-frequency noise of InP/InGaAs heterojunction bipolar transistors," *IEEE Trans. Electron Devices*, vol. 45, pp. 2400–2406, Dec. 1998.

[15] B. Bayraktaroglu, G. Dix, and D. Pavlidis, "AlGaAs/GaAs HBT reliability: Dependence on material and correlation to baseband noise," in *Tech. Dig. 19th GaAs IC Symp.*, 1997, pp. 157–160.

[16] A. K. Kirtania, M. B. Das, S. Chandrasekhar, L. M. Lunardi, G. J. Qua, R. A. Hamm, and L. W. Yang, "Measurement and comparison of $1/f$ noise and g–r noise in silicon homojunction and III–V heterojunction bipolar transistors," *IEEE Trans. Electron Devices*, vol. 43, pp. 784–792, May 1996.

[17] D. Huber, R. Bauknecht, C. Bergamaschi, M. Bitter, A. Huber, T. Morf, A. Neiger, M. Rohner, I. Schnyder, V. Schwarz, and H. Jäckel, "InP/InGaAs single HBT technology for photoreceiver OEIC's at 40 Gb/s and beyond," *J. Lightwave Technol.*, vol. 18, pp. 992–1000, July 2000.

[18] J. R. Hauser, "The effects of distributed base potential on emitter–current injection density and effective base resistance for stripe transistor geometries," *IEEE Trans. Electron Devices*, vol. ED-11, pp. 238–242, May 1964.

[19] H. H. Berger, "Models for contacts to planar devices," *Solid-State Electron.*, vol. 15, pp. 145–158, Feb. 1972.

[20] D. Ritter, R. A. Hamm, A. Feygenson, M. B. Panish, and S. Chandrasekhar, "Diffusive base transport in narrow base InP/$Ga_{0.47}In_{0.53}As$ heterojunction bipolar transistors," *Appl. Phys. Lett.*, vol. 59, pp. 3431–3433, Dec. 1991.

[21] A. Feygenson, O. A. Mezrin, P. R. Smith, R. A. Hamm, R. K. Montgomery, R. D. Yadvish, D. Ritter, and M. Haner, "Ballistic transport effects in InP/InGaAs heterostructure bipolar transistors," in *IEEE Int. Electron Device Meeting*, 1993, pp. 799–802.

[22] A. van der Ziel, "Theory of shot noise in junction diodes and junction transistors," *Proc. IRE*, pp. 1639–1646, Nov. 1955.

[23] ——, "Noise in solid-state devices and lasers," *Proc. IEEE*, vol. 58, pp. 1178–1206, Aug. 1970.

[24] L. Escotte, J. G. Tartarin, R. Plana, and J. Grafeuil, "High-frequency noise in heterojunction bipolar transistors," *Solid-State Electron.*, vol. 42, no. 4, pp. 661–663, 1998.

[25] A. Ambrózy, *Electronic Noise*. New York: McGraw-Hill, 1982.

[26] A. van der Ziel, *Noise in Solid State Devices and Circuits*. New York: Wiley, 1986.

[27] A. Ouacha, M. Willander, R. Plana, J. Graffeuil, L. Escotte, and B. Willen, "Low frequency noise characterization of self-aligned InP/InGaAs heterojunction bipolar transistor," *J. Appl. Phys.*, vol. 78, pp. 2565–2567, Aug. 1995.

[28] A. van der Ziel, "Proposed discrimination between $1/f$ noise source in transistors," *Solid-State Electron.*, vol. 25, pp. 141–143, Feb. 1982.

[29] A. Huber, C. Bergamaschi, R. Bauknecht, H. Jäckel, and H. Melchior, "Minimization of the noise measure of InP/InGaAs HBTs," in *Proc. 9th Int. Indium Phosphide Related Mater. Conf.*, 1997, pp. 649–652.

[30] A. Huber, C. Bergamaschi, T. Morf, and H. Jäckel, "Broadband noise model for InP/InGaAs HBTs," in *Proc. 10th Int. Indium Phosphide Related Mat. Conf.*, 1998.

[31] A. Huber, I. Schnyder, H. Jäckel, C. Bergamaschi, and K. Schenk, "The influence of the emitter orientation on the noise characteristics of InP/InGaAs(P) DHBT's," in *Proc. 24th Compound Semiconduct. Devices and Circuits Workshop*, 2000, pp. VII-7–VII-8.

[32] A. Huber, D. Huber, C. Bergamaschi, T. Morf, and H. Jäckel, "A lumped DC-50 GHz amplifier using InP/InGaAs HBTs," *Electron. Lett.*, vol. 35, pp. 53–55, Jan. 1999.

[33] ——, "Design and characterization of a 50 GHz InP/InGaAs HBT amplifier," in *Proc. 11th Int. Indium Phosphide Related Mater. Conf.*, 1999, pp. 191–194.

[34] I. Kipnis, J. F. Kukielka, J. Wholey, and C. P. Snapp, "Silicon bipolar fixed and variable gain amplifier MMIC's for microwave and lightwave applications up to 6 GHz," in *IEEE Microwave Millimeter-Wave Monolithic Circuits Symp. Dig.*, 1989, pp. 101–104.

[35] B. Agarwal, Q. Lee, D. Mensa, R. Pullela, J. Guthrie, and M. J. W. Rodwell, "Broadband feedback amplifier with AlInAs/GaInAs transferred-substrate HBT," *Electron. Lett.*, vol. 34, pp. 1357–1358, June 1998.

[36] Y. Suzuki, H. Shimawaki, Y. Amamiya, N. Nagano, T. Niwa, H. Yano, and K. Honjo, "50-GHz-bandwidth baseband amplifiers using GaAs-based HBTs," in *1997 IEEE GaAs IC-Symp. Dig.*.

[37] H. T. Friis, "Noise figure of radio receiver," *Proc. IRE*, vol. 32, pp. 419–422, July 1944.

[38] V. Hurm, W. Benz, W. Bronner, A. Hülsmann, T. Jakobus, K. Köhler, A. Leven, M. Ludwig, B. Raynor, J. Rosenzweig, M. Schlechtweg, and A. Thiede, "40 Gbit/s 1.55 μm PIN-HEMT photoreceiver monolithically integrated on a 3 in GaAs substrate," *Electron. Lett.*, vol. 34, pp. 2060–2061, Oct. 1998.

A. Huber (S'93–M'99), photograph and biography not available at the time of publication.

D. Huber (S'99), photograph and biography not available at the time of publication.

C. Bergamaschi (S'90–M'95), photograph and biography not available at the time of publication.

T. Morf (S'89–M'90), photograph and biography not available at the time of publication.

H. Jäckel (M'80), photograph and biography not available at the time of publication.